

# Realization of a chip-based hybrid trapping setup for $^{87}\text{Rb}$ atoms and $\text{Yb}^+$ Ion crystals

A. Bahrami<sup>1,2</sup> and F. Schmidt-Kaler<sup>2</sup>

<sup>1</sup>*Department of Electrical and Computer Engineering, University of California, Los Angeles, Los Angeles, CA 90095, USA*

<sup>2</sup>*Institut für Physik, Johannes Gutenberg-Universität Mainz, Mainz D-55099, Germany*

(\*Electronic mail: abasalt@ucla.edu.)

(Dated: 9 January 2024)

Hybrid quantum systems integrate laser-cooled trapped ions and ultracold quantum gases within a single experimental configuration, offering vast potential for applications in quantum chemistry, polaron physics, quantum information processing, and quantum simulations. In this study, we introduce the development and experimental validation of an ion trap chip that incorporates a flat atomic chip trap directly beneath it. This innovative design addresses specific challenges associated with hybrid atom-ion traps by providing precisely aligned and stable components, facilitating independent adjustments of the depth of the atomic trapping potential and the positioning of trapped ions. Our findings include successful loading of the ion trap with linear  $\text{Yb}^+$  ion crystals and the loading of neutral  $^{87}\text{Rb}$  atoms into a mirror magneto-optical trap (mMOT).

## I. INTRODUCTION

To advance in the field of hybrid quantum systems, we employ a combination of trapping methods for atomic ions and neutral atoms. The trapped ions provide highly controllable quantum systems, making them a valuable platform for a wide range of applications, including quantum information<sup>1,2</sup>, high-resolution spectroscopy, and tests of fundamental physics<sup>3</sup>. On the other hand, interactions between neutral atoms primarily result from short-range van der Waals forces, which range from one to several angstroms.

Atomic ions are confined in Paul traps<sup>4,5</sup>. These traps employ a radio frequency (RF) quadrupolar field to create a harmonic trapping potential. In linear Paul traps, this quadrupolar field is extended along a line, and additional electrodes are used to precisely control of the ion crystal position and shape. Neutral atoms have been confined using various techniques such as magneto-optical traps (MOT)<sup>6</sup>, magnetic quadrupolar fields<sup>7</sup>, or far-detuned laser light<sup>8</sup>. We are combining different trapping methods to build the device for a hybrid atom-ion system to exploit its unique properties. The temperature of a confined atomic cloud can be reduced by combinations of laser and evaporation cooling to nanokelvin, even pico Kelvin range, while the temperature of Doppler cooled trapped ions is about a milli Kelvin, advanced cooling techniques may reach a few tenths of micro Kelvin. Sympathetic cooling an ion crystal by means of thermalization with atoms was one of the early motivations for such hybrid systems<sup>9-11</sup>. However, the RF-driven motion of a trapped ion during the interaction with the neutral atom, a short-range (Langevin) collision, leads to heating. Research has shown that the lowest temperatures can be reached for the largest ion-atom mass ratios  $m_i/m_a$ <sup>12</sup>. The  $\text{Yb}^+/\text{Li}$  hybrid system with a mass ratio of  $m_i/m_a \approx 29$  may be considered optimum to minimize that adverse effect. For other combinations of atoms and ions, such as  $\text{Rb}/\text{Ba}^+$ ,  $\text{Rb}/\text{Rb}^+$ ,  $\text{Rb}/\text{Yb}^+$ ,  $\text{Rb}/\text{Sr}^+$ , ect. where short-range collision-induced heating has prohibited to enter low energy scattering regimes.

We present a chip-based hybrid trapping device as a novel tool to largely avoid collision-induced heating for any combination of atom and ion. Two properties are key: first, the device integrates a linear Paul trap where ions crystals may be positioned accurately with respect to a Ioffe-Pritchard (IP) magnetic trap that confines an atomic sample. Second, chip-based atom or ion traps feature tightly confining potentials such that both, such that the ion crystal may be positioned *close*, but not directly on the atomic sample. In such way, one may explore interactions at mutual distances of a  $\mu\text{m}$ , but short-range collision-induced heating is mitigated.

Here, we describe a device for a combination of Rb atoms and  $\text{Yb}^+$  ions<sup>13</sup>. After giving an overview of the entire device, we are describing the ion chip, then the atom chip trap, followed by a short description of laser systems to cool the ions and atoms, and optics to detect their laser induced fluorescence. The planar Paul trap chip is sitting directly on top of the atom chip trap device. We show the operation of the planar segmented ion trap with a linear ion crystal<sup>14</sup>. Also we demonstrate the operation of a mMOT<sup>15</sup>, to load the atomic chip trap which features u- and z-shaped wires for versatile magnetic trapping situations.

## II. SYSTEM OVERVIEW

Our experimental setup is a hybrid atom-ion chip trap designed to capture and manipulate both laser-cooled neutral  $^{87}\text{Rb}$  atoms and  $\text{Yb}^+$  ions. This system allows for controlled investigations into the interactions of these particles in a precisely defined environment.

The experimental setup comprises an atom chip designed for trapping neutral  $^{87}\text{Rb}$  atoms. This chip incorporates an mMOT for loading and cooling, current-carrying wires for atom transport, and a magnetic trap (MT) for the final confinement of atoms (Fig. 1). Additionally, a surface electrode ion trap (Fig. 3) is employed for trapping  $\text{Yb}^+$  ions. Underneath the atom chip we have implemented a big u-shaped wire

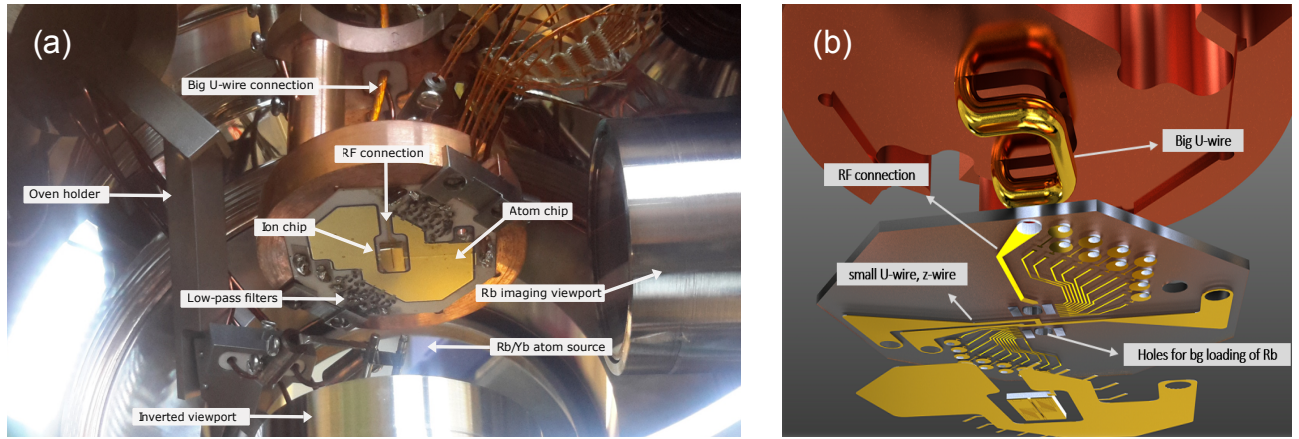


FIG. 1. A visual representation of our experimental setup when installed within an ultra-high vacuum (UHV) chamber (a). The overall dimensions of the chip are 45 mm in outer diameter and 1 mm in total height. As the trapping area is limited by the surface of the ion trap at a position of 0.6 mm, the trap depth is estimated to be  $273 \mu\text{K}$ . (b) presents an exploded view of the atom-ion chip assembly, incorporating small u- and z-shaped wires for transferring and confining the mMOT in the final stage. The z-shaped wire has a height of 0.08 mm and width of 0.6 mm.

essential for capturing atoms in a secondary mMOT (Fig. 1b). The atom chip also features small wires with two distinct geometries: a u-shaped configuration designed to compress and transfer atoms from the second mMOT to the ion trapping region, and a z-shaped wire designed for trapping atoms in MT. The atom chip itself is fabricated using thick film technology, enabling the printing of UHV compatible, sub-millimeter scale electrical circuits on an alumina substrate ( $\text{Al}_2\text{O}_3$ ). Additionally, the atom chip incorporates a filter board for the direct current control electrodes of the ion trap, which incorporates 3.38 MHz low-pass filters (with capacitance of 4.7 nF and resistance of  $10 \Omega$ ) for all DC electrodes to mitigate RF pickups in proximity to the ion trap.

After capturing atoms in the mMOT (Fig. 2a), the mMOT coils switch to a bias field while activating the large u-shaped wire beneath the atom chip (Fig. 2b). As a result, the atoms can be confined approximately 2-5 mm below the ion chip surface within a smaller spatial area.

Following this, the atoms are transferred to a potential created by the small u-shaped wire on the atom chip (Fig. 2c). During this process, we move the atoms close to the ion trap surface, compressing the atom cloud into a smaller and steeper mMOT volume<sup>16</sup>. In the final step, an IP trap is established by turning on the z-shaped wire (Fig. 5) on the atom chip along with a bias magnetic fields.  $^{174}\text{Yb}^+$  ions are loaded into the ion trap, creating a shared volume where the interactions between the atoms and ions can be studied in detail. To maintain the required low pressure, we employ an ion getter pump, ensuring a stable experimental environment with pressures as low as  $1.3 \times 10^{-9}$  mBar.

The setup should allow us to trap  $^{87}\text{Rb}$  atoms which will be evaporated from an alkali metal dispensers with temperatures of about  $750^\circ\text{C}$  and to cool them down to  $T_D = 140 \mu\text{K}$ . The final trap frequencies for trapped atoms are  $\omega/2\pi \sim (1.17, 1.17, 0.08)$  kHz.

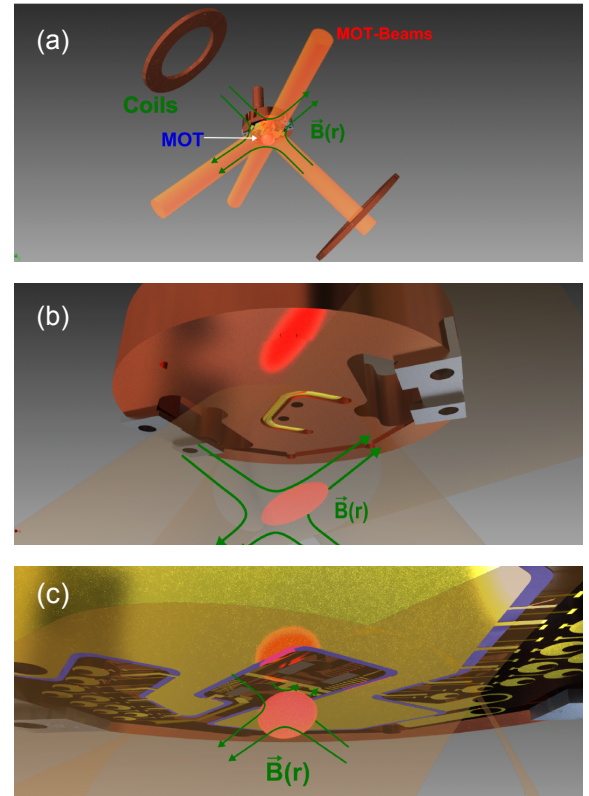


FIG. 2. (a) An mMOT is created using  $\sigma^\pm$  light beams and a magnetic quadrupole field generated by two coils carrying current in an anti-Helmholtz configuration. (b) The quadrupole field for the mMOT is produced by the magnetic field of a big u-shaped wire carrying current beneath the chip, combined with a uniform bias field. (c) On the chip, small u-shaped wire forms a more compact and steeper quadrupole field directly above the ion trap.

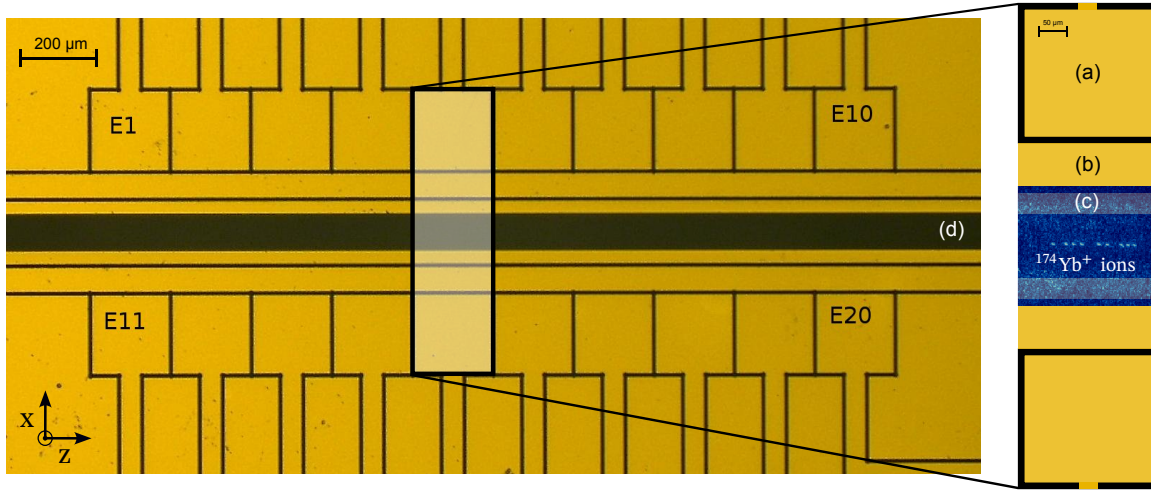


FIG. 3. The image above is a magnified optical microscope image of the microfabricated surface trap used in our experimental setup. It features 21 static voltage electrodes, including 20 with a size of  $200 \times 200 \mu\text{m}^2$  (a), which are used for radial confinement (E01 - E20), one long, symmetric F-shaped rail for RF confinement (b) and one inner compensation electrode (c), which extends axially and symmetrically along a slit of  $100 \mu\text{m}$  width and  $5 \text{ mm}$  length (d). This slit is employed to load Rb atoms from the dispenser positioned directly behind the ion trap. In the experiments described here,  $\text{Yb}^+$  ion crystals are trapped and confined along the trap axis (z-direction). The CCD image, captured with an exposure time of  $1.3 \text{ s}$ , depicts nine  $^{174}\text{Yb}^+$  ions in a linear crystal that is trapped with corresponding trap frequencies of  $(\omega_x, \omega_z)/2\pi = (406, 110) \text{ kHz}$ .

### III. ION TRAP DESCRIPTION

This ion trap is a microfabricated surface electrode segmented design with a trapping height of  $100 \mu\text{m}$ . The dimensions of the chip are  $9 \text{ mm}$  in length,  $4.5 \text{ mm}$  in width, and  $500 \mu\text{m}$  in thickness. This chip includes a slit of a  $100 \mu\text{m}$  wide and  $6.5 \text{ mm}$  long, positioned just below the ion trapping region. This slit will function as the entry point for loading atoms using an atomic dispenser.

The fabrication process of this chip follows these steps: The electrode structure is etched onto a fused silica substrate using a combination of laser weakening and HF etching. Subsequently, four metal layers are evaporated onto the substrate. These metal layers consist of  $20 \text{ nm}$  of Titanium,  $150 \text{ nm}$  of gold, another  $20 \text{ nm}$  of Titanium, and an additional  $150 \text{ nm}$  of gold<sup>17</sup>. The chip structure comprises 21 DC electrodes labeled as E1 to E21, along with one RF electrode (RF), while the rest of the surface remains grounded. The isolation between the electrodes is approximately  $10 \mu\text{m}$  wide and  $50 \mu\text{m}$  deep, which is large enough to prevent electrical breakdown at  $100\text{-}200 \text{ V}_{pp}$ . To provide the voltage for the DC electrodes, we use FPGA-controlled digital-to-analog conversion (DAC) boards<sup>18</sup>. It supports up to 48 independent analog channels (16 bits) and 25 digital TTL signals per unit. Analog channels have a voltage range of  $-10 \text{ V}$  to  $+10 \text{ V}$  with a resolution of  $0.12 \text{ mV}$  per least significant bit (LSB).

The ion trap is glued to the center of the atom trap using a UV-curable adhesive. To establish the necessary electrical connections from the filter board to the ion trap, a wire bonder (HB10) is used. The atom chip is coated with a top layer of gold, which serves as a protective layer for the wires as well as a reflecting mirror for the mMOT laser beams. Typically, we trap  $\text{Yb}^+$  ions at a distance of  $100 \mu\text{m}$  from the trap surface,

with the ability to position them axially with an accuracy of  $\pm 80 \text{ nm}$ .

### IV. ATOM TRAPS

Magnetic trapping of atoms involves employing magnetic fields to confine and manipulate atoms. One common technique is the use of a quadrupole magnetic trap, established by employing two coils with currents flowing in opposite directions<sup>19</sup>. However, quadrupole trap has a zero minimum at the origin and significant limitation of this traps is the loss of cold atoms from the trap due to nonadiabatic *spin-flip Majorana transition*<sup>20</sup>. This problem has been addressed through the implementation of time-averaged orbiting potential (TOP) traps<sup>21</sup> and IP magnetic traps<sup>22</sup>. The TOP trap operates by leveraging the time-averaging of an adiabatically modulated trapping potential. In this approach, the potential is varied slowly to ensure adiabatic conditions, allowing for the stable trapping of neutral atoms. Conversely, the IP trap relies on a combination of static and radiofrequency (RF) magnetic fields to create a three-dimensional trapping potential. The RF field is typically employed for radial confinement, while the static field contributes to axial confinement.

To create a mMOT, we used right-hand circular (RHC) and left-hand circular (LHC) polarized light to drive the  $\sigma^+$  and  $\sigma^-$  transitions (Fig. 4). To trap and cool atoms we used two home-made external cavity diode lasers (ECDLs) that have a minimum output power of  $130 \text{ mW}$  under continuous wave conditions (LNC728PS01WW). Each laser is individually frequency-stabilized to the atomic transitions in  $^{87}\text{Rb}$ 's D2 line with a natural linewidth of  $\Gamma \approx 2\pi \times 6.0 \text{ MHz}$ <sup>23</sup>. These lasers provide the necessary cooling, red-detuned from

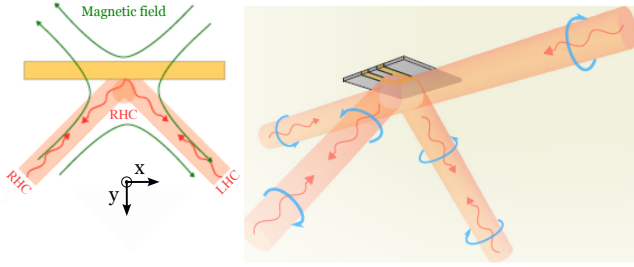


FIG. 4. Laser beams (red) with RHC and LHC laser lights to run the  $\sigma^+$  and  $\sigma^-$  transitions with a quadrupole magnetic field (green). The gold-coated surface of the atom trap is depicted by the yellow rectangle.

$|F = 2\rangle \rightarrow |F' = 3\rangle$  resonant transition, and repump laser frequencies,  $|F = 1\rangle \rightarrow |F'\rangle$  resonant transition, for the experiment.

The atom trap chip features two primary trapping wires: a small u- and a z-shaped (Fig. 5). During the final trapping stage with the z-shaped wire, for a field zero-minimum at  $(x = 0, y = 0.7, z = 0)$  mm, we applied bias fields of  $\mathbf{B}_{\text{bias}} = -\mathbf{B}_{z\text{-wire}}(0, 0.7, 0) = (30.3, 0, -21.2)$  G. To avoid Majorana spin flips, we will apply another external field  $B_z$  in the direction of the trapping wire to raise the minimum of the field to non-zero, to achieve the adiabatic limit. The external field  $B_z = 0.5$  G together with  $\mathbf{B}_{\text{bias}}$  form an IP trap with a non-zero minimum<sup>13</sup>.

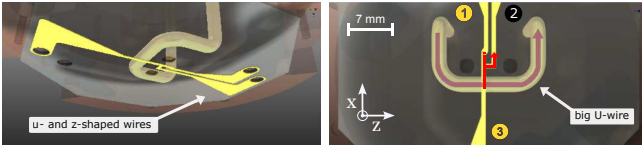


FIG. 5. Small u- and z-shaped wires to compress and confine atoms in an IP trap. Grounded at (2), we pass current through (1) to generate u-shaped wire potential and through (3) for the z-shaped wire potential. Red arrows illustrate the flow of electric currents.

The axial orientation of the atom cloud confined within the IP trap may not align perfectly with the z-axis<sup>24</sup>. In the design of the atom trap, we have taken into account a z-shaped wire length of  $s = 1.4$  mm, ensuring significant overlap between the atom cloud and the ion cloud (Fig. 6).

### A. Quadrupole magnetic field

The quadrupole magnetic field needed for the mMOT must be specifically engineered. A field that increases in strength as the distance from its center increases is necessary. Here, we discuss the design of a quadrupole magnetic field using two coils in an anti-Helmholtz configuration (Fig. 7). We constructed a set of MOT coils using hollow-core copper wire with a cross-sectional area of  $6 \times 6 \text{ mm}^2$  (inner cross-sectional area  $4 \times 4 \text{ mm}^2$ ). To ensure proper insulation between the wires, they were wrapped twice in Kapton tape. Each coil

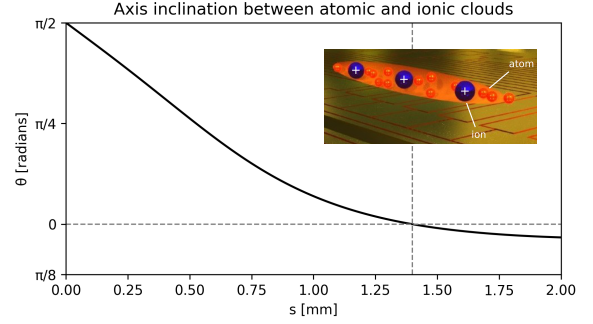


FIG. 6. Angle  $\theta$  between the z-axis of the ion trap and the axial direction of the atom trap potential versus the length of the z-shaped wire along z-direction at trapping height of 0.70 mm. At  $\theta=0$ , ions represented by blue spheres, are immersed within the atom cloud.

comprises 36 turns and has an internal diameter of 77.60 mm and an external diameter of 149.60 mm. During MOT operation, the maximum current ( $I = 200$  A) provided by a power supply (SM 30-200) flows through the wires of the coils. The current, denoted as  $I$ , produces a magnetic field gradient of  $0.059 \times I$  (G/cm) in the axial direction and  $0.029 \times I$  (G/cm) in the radial direction near the trap center.

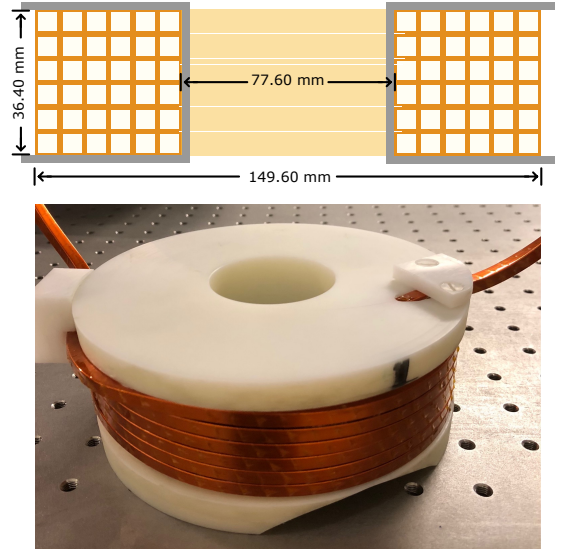


FIG. 7. Sketch of one of the MOT coils. Each coil comprises  $6 \times 6$  turns made of a hollow-core copper wire with an outer and inner cross-sectional area of  $6 \times 6 \text{ mm}^2$  and  $4 \times 4 \text{ mm}^2$ . The photograph below showcases a fabricated MOT coil.

To estimate the thermal budget of the coils, we calculated the volumetric flow rate of the cooling water which is an incompressible liquid<sup>25</sup>. The maximum pressure drop in our chiller is 4.5 bar (MINORE 0-RB400). With a pressure loss of about 0.5 bar, we estimate a temperature increase of about 2-4 °C, which is in close agreement with the measured temperature increase when the MOT coils were running continuously at  $I = 200$  A. At this current, the energy dissipated in each coil

TABLE I. Details of the individual MOT coils' production.

Quantity	Value	Unit
Number of winding	36	
Cross-section area	20.0	$\text{mm}^2$
Coil length	11.99	m
Coil mass	2.14	Kg
Water mass	0.19	Kg
Coil resistance	10.0	$\text{m}\Omega$
Power dissipation	419.0	W
Voltage drop	2.05	V
Pressure drop	0.5	bar
Volumetric flow rate	2.36	l/min
Water mass flow rate	2.35	Kg/min
Fluid velocity	2.46	m/s
Reynolds number	2575.4	-
Temperature rise	2.5	$^\circ\text{C}$

is approximately 900 W and the voltage loss 4.15 V. The voltage loss increases to 7.0 V when we engage the MOT switch (Fig. 8).

### B. Fast switch for MOT coil

Fast magnetic field switching is essential for maintaining the stability of the MOT, enhancing the laser cooling efficiency, and for performing various manipulation of trapped atoms. However, doing so caused eddy currents to form in the electrical conductive parts, leading to a slow decay of the magnetic field. To solve this issue, we implemented a Polyoxymethylene holder for the coils. To achieve fast switching, we developed a current driver using high-speed insulated gate bipolar transistors (IGBTs). We used a series connection of  $10 \times 5$  transient-voltage-suppressor diodes (TVS diodes) followed by a resistor (Fig. 8). Each diode has a breakdown voltage of 100 V, allowing the magnetic energy to dissipate to ground as soon as the reverse voltage reaches 500 V. With this setup, we succeeded in achieving a switching-off time less than  $100 \mu\text{s}$  for 200 A. We observed a linear relationship between the applied current in the magnetic trap coils and the switching-off time, with a rate of  $0.45 \mu\text{s}$  per 1 A.

## V. ION TRAPPING

Trapping, cooling and imaging of  $\text{Yb}^+$  ions requires three lasers. The ionization of Yb atom is done via a two level scheme. A laser at 398.9 nm excites the neutral Yb atom to the  $^1\text{P}_1$  state. The second step is done with a laser at 369 nm, which ionizes the Yb atom. The same laser beam is used to doppler cool and image the ion. This laser drives the  $^2\text{S}_{1/2} \leftrightarrow ^2\text{P}_{1/2}$  dipole transition. In 0.5% of the decays the ion falls into meta stable  $^2\text{D}_{3/2}$  state. To bring the ion back to the cooling cycle a repump laser at 935 nm is used<sup>13</sup>.

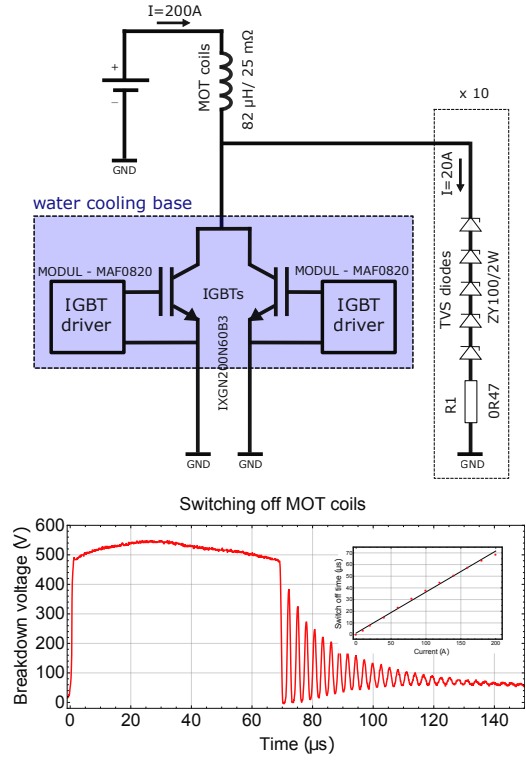


FIG. 8. The circuit diagram for high-speed IGBT-driven current switching. The MOT coils are connected in series, resulting in a total electrical inductance of  $82 \mu\text{H}$  and a resistance of  $25 \text{m}\Omega$ . When the maximum current of 200 A is switched off, an electromotive force is generated that triggers the transient-voltage-suppression diodes.

The blue lasers are overlapped and directed into a UV polarization-maintaining (PM) fiber, while the repump laser is coupled to an infrared (IR) PM fiber. Subsequently, all beams are combined using a dichroic mirror (Thorlabs M254C45), which reflects UV light and transmits IR light. A 200 mm focal length achromatic lens is placed behind the dichroic mirror to focus the beams parallel to the ion chip surface in the ion trapping region, positioned around  $100 \mu\text{m}$  beneath the ion chip. The focal sizes of the UV beams at this location are  $30 \mu\text{m}$ , and the repump beam has a focal size of  $100 \mu\text{m}$ . The angle of incidence with respect to the ion-chip  $z$ -axis is  $10^\circ$ , enabling ion cooling in both radial and axial directions. Effective ion cooling is achieved by applying DC voltages to the DC electrodes E01-E20 (Fig. 3) and rotating the principal axes of the trap<sup>13</sup>.

After trapping ions, we used transverse confinement to arrange the trapped ions into a linear crystal. A gradual reduction in trap anisotropy triggers a structural phase transition, transforming the arrangement from linear to a zigzag configuration (Fig. 9).

The lifetime of a Doppler cooled single ions are about 2 min. Excessive micromotion amplitude can be addressed through various methods<sup>27–30</sup>. When a laser is red-detuned near the natural linewidth of the atom, the ion fluorescence rate increases with decreasing micromotion amplitude, particularly for low magnitudes of micromotion. After the 2D com-

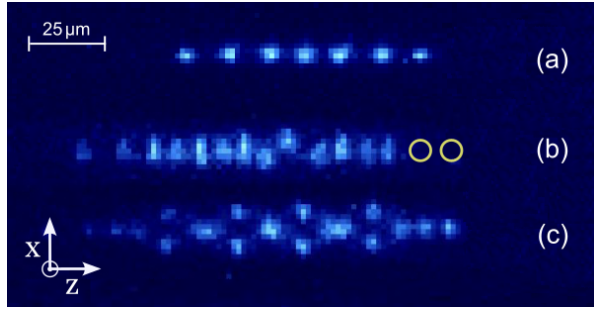


FIG. 9. (a) Crystal of eight  $^{174}\text{Yb}^+$  ions, (b) and (c) Zig-zag configuration of  $^{174}\text{Yb}^+$  ions<sup>26</sup>. By examining the positions of individual ions, we notice two dark  $\text{Yb}^+$  ions enclosed in yellow circles. Each pixel in the image corresponds to  $1.09 \pm 0.07 \mu\text{m}$ .

compensation, we measured a residual electric stray field uncertainty of  $(\Delta\epsilon_x, \Delta\epsilon_z) = (0.76, 0.45) \text{Vm}^{-1}$  at a trap frequency of  $(\omega_x, \omega_z)/2\pi = (426, 260) \text{kHz}$ . This micromotion compensation is good enough for the initial studies of atom-ion interaction<sup>31</sup>.

## VI. ATOMS TRAPPED IN mMOT

Trapping atoms beneath the atom-ion chip is particularly challenging because the reflection of beams off the traps leads to changes in light polarization, alterations in beam quality, and variations in intensity. Initially we tested the mMOT in a test setup with just a gold mirror (Thorlabs PF20-03-M03) instead of original trap. We aligned all the laser beams with the zero of the quadrupole magnetic field and trapped a mMOT directly from the background vapor of the atoms. Under our typical experimental conditions, 13 G/cm axial magnetic field gradient and laser detuning of  $\Delta \approx -\Gamma/2$ , we capture atomic cloud with an approximate radius of  $r = (1.8 \pm 0.20) \text{mm}$  that contains roughly  $N = (2.3 \pm 0.3) \times 10^8$  atoms of  $^{87}\text{Rb}$ . These values are determined from fluorescence signals (Fig. 10).

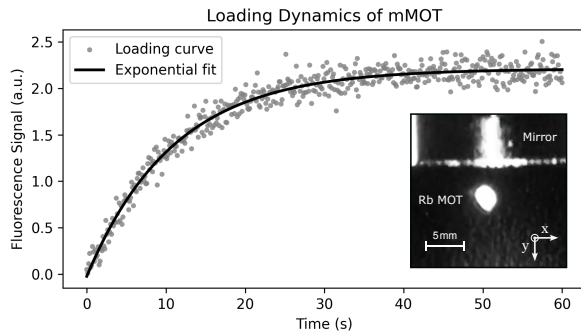


FIG. 10. The dynamics of  $^{87}\text{Rb}$  atoms confined in a mMOT with a 13 G/cm axial magnetic gradient. The solid line is the exponential fit to the measurements taken within a UHV chamber at a pressure of  $1.3 \times 10^{-9} \text{mbar}$ . The bright spot in the center is the  $^{87}\text{Rb}$  MOT, and above this, the side of the gold-coated mirror is visible. The cooling laser beam intensity and detuning are  $6.5 \text{mW/cm}^2$  and  $-12 \text{MHz}$  respectively used in these experiments.

The fluorescence intensity emitted from trapped atoms in the MOT is proportional to the number of atoms. The dynamics of atoms loading into a MOT can be described by<sup>32,33</sup>:

$$\frac{dN(t)}{dt} = R - \gamma N(t) - \beta \bar{n} N(t). \quad (1)$$

Here,  $N$  represents the atom count,  $R$  signifies the loading rate of atoms,  $\gamma$  denotes the loss rate resulting from spontaneous emission, and  $\beta$  accounts for the loss rate due to collisions with the background gas. The density of the background gas is represented as  $\bar{n}$ . In the constant background gas density limit, Eq. 1 simplifies to:

$$N(t) = \frac{R}{(\gamma + \beta \bar{n})} (1 - e^{-(\gamma + \beta \bar{n})t}) = \frac{R}{\zeta} (1 - e^{-\zeta t}). \quad (2)$$

We simplified Eq. 2 by substituting  $\gamma + \beta \bar{n} = \zeta$ . By analyzing the loading curves of a mMOT as shown in Fig. 10, one can determine the values of  $R$  and  $\zeta$ . In our case, we typically obtain a ratio of  $R/\zeta = (2.0 \pm 0.3) \times 10^8$  and a value of  $\zeta = 0.09 \pm 0.01 \text{s}^{-1}$ .

### A. Big u-shaped wire trap

Subsequently, we positioned the atom-ion trap inside the UHV chamber. We observed a 15% reduction in the intensity of beams reflected from the ion trap surface due to microfabricated structures on the chip. This imbalance in optical pressures results in a slight shift of the atom trapping location away from the zero point of the quadrupole magnetic field. However, the beam diameter (5-10 mm) is sufficient to offset this effect. Following the recapturing of the mMOT beneath the ion-chip, we turned on the big u-wire potential by applying 15 A (Fig. 5).

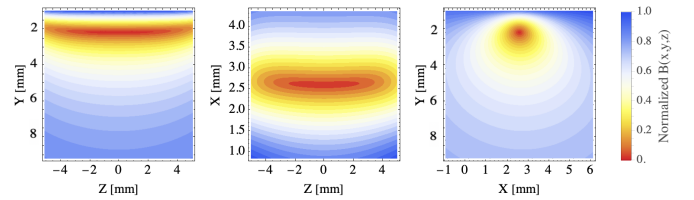


FIG. 11. The zero-minimum magnetic field potential at  $(2.6, 2, 0) \text{mm}$  is generated by the big u-shaped wire carrying a current of  $I = 15 \text{A}$ , along with bias fields of  $\mathbf{B}_{\text{bias}} = (10.3, 2.2, 0) \text{G}$ .

In order to establish a field minimum at the coordinates  $(x = 2.6, y = 2, z = 0) \text{mm}$ , we applied bias fields  $\mathbf{B}_{\text{bias}} = -\mathbf{B}_{\text{u-wire}}(2.6, 2, 0) = (10.3, 2.2, 0) \text{G}$  (Fig. 11). This results in a magnetic field gradient of  $\nabla \mathbf{B} = (4.8, -4.7, -0.1) \text{G/mm}$ . To increase the intensities of the MOT beams, we decreased the beam diameter from 10 mm to 5 mm and trapped a relatively small atomic cloud positioned 2 mm below the ion trap chip (Fig. 12). At this position, the trapped atoms and ions are

not yet spatially overlapped. The subsequent step involves optimizing the transfer of atoms from this location to the small u-shaped and ultimately z-shaped potentials.

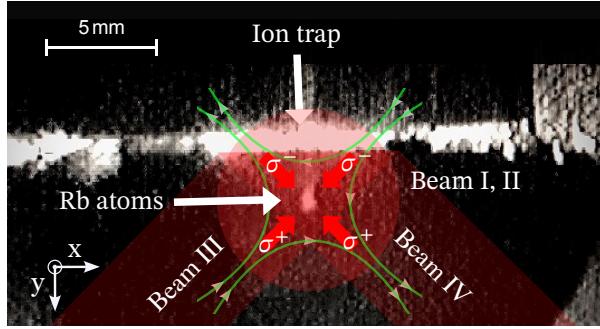


FIG. 12. Image of the  $^{87}\text{Rb}$  mMOT under the ion trap chip. Beams I and II (directed toward/away from the page), and III are all RHC polarized, while beam IV is LHC polarized. The green lines depict the quadrupole magnetic field lines of the trapping potential created by big u-wire. The ion trap, with a width of  $w = 5$  mm, is also visible due to light reflections.

A primary objective of this experiment is to investigate the interactions of atoms with ions through induced dipole moments. To this end, it is crucial to establish a characteristic range of the atom-ion interaction, which is defined by the length scale  $R^* = \sqrt{2C_4/\hbar^2}$ . Here,  $R$ , the characteristic range, is determined by the constant  $C_4$  related to induced dipole moments and the reduced Planck's constant  $\hbar$ .

For these interactions, the ionic wave packet length  $l_a = \sqrt{\hbar/m_a\omega_a}$  must be proportional with  $R$ , where  $l_a$  represents the ionic wave packet length,  $m_a$  the mass of the ions, and  $\omega_a$  the trap frequency for the ions. The specific mixture of  $^{174}\text{Yb}^+$  and  $^{87}\text{Rb}$  atoms used in this experiment results in  $R^* = 306$  nm, requiring a trap frequency of 1.23 kHz. The corresponding single atom wave packet sizes are  $l_a = (315, 315, 1175)$  nm. In contrast to traditional hybrid trap designs<sup>34</sup>, this particular trap design offers improved trapping stability and a streamlined infrastructure, making it an ideal foundation for further advancements.

Having successfully integrated cooling and trapping techniques for atoms and ions on a single microfabricated chip, the subsequent phase involves confining the atoms in a MT to study atom-ion interactions. At low energy levels, two-body collisions between a hetero-nuclear ion  $A^+$  and an atom  $B$  can result in various processes. These include elastic collisions where the internal states of both the atom and ion remain unchanged<sup>35</sup>. Furthermore, spin exchange within the ion-atom pair is a potential occurrence<sup>36</sup>. Additionally, in close proximity, an electron from atom  $B$  may transition to  $A^+$ , initiating a charge transfer process<sup>37,38</sup>.

## VII. CONCLUSION

The hybrid atom-ion system we have introduced facilitates the exploration of Josephson physics. Using an atom-ion

setup allows for the investigation of tunneling phenomena in a double well potential. The control over tunneling dynamics is achieved through manipulation of the internal state of the ion<sup>39</sup>. In scenarios where a crystal of ions is coupled to an atomic cloud, the ions organize into lattices, imparting a band structure onto the atoms. This coupling enables the exploration of various quantum phenomena, such as polaron physics and Peierls transitions<sup>40</sup>. Furthermore, the detection of a magnetic field gradient induced by the magnetic dipole of a single atom becomes feasible with a single ion positioned nearby<sup>41</sup>.

## ACKNOWLEDGMENTS

We acknowledge the scientific contributions of Rene Gerritsma, Matthias Müller and Jannis Joger into the project. Our thanks go to Hartmut Häffner and his team for providing the trap chip. We express special thanks to the SFB/TR49 for their generous financial support.

## AUTHOR DECLARATIONS

### Conflict of Interest

The authors have no conflicts to disclose.

## DATA AVAILABILITY

The data that support the findings of this study are available from the corresponding author upon reasonable request.

## REFERENCES

- <sup>1</sup>H. Häffner, C. Roos, and R. Blatt, "Quantum computing with trapped ions," *Physics Reports* **469** (2008).
- <sup>2</sup>K. Singer, U. Poschinger, M. Murphy, P. Ivanov, F. Ziesel, T. Calarco, and F. Schmidt-Kaler, "Colloquium: Trapped ions as quantum bits: Essential numerical tools," *Rev. Mod. Phys.* **82** (2010).
- <sup>3</sup>M. S. Safronova, D. Budker, D. DeMille, D. F. J. Kimball, A. Derevianko, and C. W. Clark, "Search for new physics with atoms and molecules," *Rev. Mod. Phys.* **90**, 025008 (2018).
- <sup>4</sup>P. Wolfgang, "Ein Ionenkäfig," in *Forschungsberichte des Wirtschafts- und Verkehrsministeriums Nordrhein-Westfalen*, Vol. 415 (VS Verlag für Sozialwissenschaften, Wiesbaden, 1958).
- <sup>5</sup>M. G. Raizen, J. M. Gilligan, J. C. Bergquist, W. M. Itano, and D. J. Wineland, "Linear trap for high-accuracy spectroscopy of stored ions," *Journal of Modern Optics* **39**, 233–242 (1992), <http://dx.doi.org/10.1080/09500349214550241>.
- <sup>6</sup>A. L., "First observation of magnetically trapped neutral atoms," *Phys. Rev. Lett.* **54**, 2596–2599 (1985).
- <sup>7</sup>D. E. Pritchard, "Cooling neutral atoms in a magnetic trap for precision spectroscopy," *Physical Review Letters* **51**, 1336–1339 (1983).
- <sup>8</sup>S. J. M. Kuppens, "Loading an optical dipole trap," *Physical Review A* **62** (2000), 10.1103/PhysRevA.62.013406.
- <sup>9</sup>M. Krych and Z. Idziaszek, "Description of ion motion in a paul trap immersed in a cold atomic gas," *Phys. Rev. A* **91**, 023430 (2015).
- <sup>10</sup>C. Zipkes, S. Palzer, L. Ratschbacher, C. Sias, and M. Köhl, "Cold heteronuclear atom-ion collisions," *Phys. Rev. Lett.* **105**, 133201 (2010).

- <sup>11</sup>Z. Meir, T. Sikorsky, R. Ben-shlomi, N. Akerman, Y. Dallal, and R. Ozeri, "Dynamics of a ground-state cooled ion colliding with ultra-cold atoms," *Phys. Rev. Lett.* **117**, 243401 (2016).
- <sup>12</sup>M. Cetina, A. T. Grier, and V. Vuletić, "Micromotion-induced limit to atom-ion sympathetic cooling in Paul traps," *Phys. Rev. Lett.* **109**, 253201 (2012).
- <sup>13</sup>A. Bahrami, M. Müller, M. Drechsler, J. Joger, R. Gerritsma, and F. Schmidt-Kaler, "Operation of a microfabricated planar ion-trap for studies of a  $\text{yb}^+ - \text{rb}$  hybrid quantum system," *physica status solidi (b)* **256**, 1800647 (2019).
- <sup>14</sup>J. Chiaverini, R. B. Blakestad, J. Britton, J. D. Jost, C. Langer, D. Leibfried, R. Ozeri, and D. J. Wineland, "Surface-electrode architecture for ion-trap quantum information processing," (2005), arXiv:quant-ph/0501147 [quant-ph].
- <sup>15</sup>J. Reichel, W. Hänsel, and T. W. Hänsch, "Atomic micromanipulation with magnetic surface traps," *Phys. Rev. Lett.* **83**, 3398–3401 (1999).
- <sup>16</sup>W. Petrich, M. H. Anderson, J. R. Ensher, and E. A. Cornell, "Behavior of atoms in a compressed magneto-optical trap," *JOSA B* **11**, 1332–1335 (1994).
- <sup>17</sup>M. Hellwig, A. Bautista-Salvador, K. Singer, G. Werth, and F. Schmidt-Kaler, "Fabrication of a planar micro penning trap and numerical investigations of versatile ion positioning protocols," *New Journal of Physics* **12**, 065019 (2010).
- <sup>18</sup>A. Walther, F. Ziesel, T. Ruster, S. T. Dawkins, K. Ott, M. Hettrich, K. Singer, F. Schmidt-Kaler, and U. Poschinger, "Controlling fast transport of cold trapped ions," *Physical review letters* **109**, 080501 (2012).
- <sup>19</sup>T. Esslinger, I. Bloch, and T. W. Hänsch, "Bose-einstein condensation in a quadrupole-iodine-configuration trap," *Physical Review A* **58**, R2664 (1998).
- <sup>20</sup>K. B. Davis, M.-O. Mewes, M. A. Joffe, M. R. Andrews, and W. Ketterle, "Evaporative cooling of sodium atoms," *Physical review letters* **74**, 5202 (1995).
- <sup>21</sup>W. Petrich, M. H. Anderson, J. R. Ensher, and E. A. Cornell, "Stable, tightly confining magnetic trap for evaporative cooling of neutral atoms," *Physical Review Letters* **74**, 3352 (1995).
- <sup>22</sup>U. Ernst, A. Marte, F. Schreck, J. Schuster, and G. Rempe, "Bose-einstein condensation in a pure ioffe-pritchard field configuration," *Europhysics Letters* **41**, 1 (1998).
- <sup>23</sup>U. Volz and H. Schmoranzler, "Precision lifetime measurements on alkali atoms and on helium by beam-gas-laser spectroscopy," *Physica Scripta* **1996**, 48 (1996).
- <sup>24</sup>R. Gerritsma and R. Spreuw, "Topological constraints on magnetostatic traps," *Physical Review A* **74**, 043405 (2006).
- <sup>25</sup>R. Cornish, "Flow in a pipe of rectangular cross-section," *Proceedings of the Royal Society of London. Series A, Containing Papers of a Mathematical and Physical Character* **120**, 691–700 (1928).
- <sup>26</sup>M. Müller, *Cold Rb-Yb mixtures in a hybrid trap setup*, Ph.d. thesis, Johannes Gutenberg-Universität Mainz (To be published).
- <sup>27</sup>S. Narayanan, N. Daniilidis, S. Möller, R. Clark, F. Ziesel, K. Singer, F. Schmidt-Kaler, and H. Häffner, "Electric field compensation and sensing with a single ion in a planar trap," *Journal of Applied Physics* **110** (2011).
- <sup>28</sup>D. Berkeland, J. Miller, J. C. Bergquist, W. M. Itano, and D. J. Wineland, "Minimization of ion micromotion in a paul trap," *Journal of applied physics* **83**, 5025–5033 (1998).
- <sup>29</sup>U. Tanaka, K. Masuda, Y. Akimoto, K. Koda, Y. Ibaraki, and S. Urabe, "Micromotion compensation in a surface electrode trap by parametric excitation of trapped ions," *Applied Physics B* **107**, 907–912 (2012).
- <sup>30</sup>D. Allcock, T. Harty, H. Janacek, N. Linke, C. Ballance, A. Steane, D. Lucas, R. Jarecki, S. Habermehl, M. Blain, *et al.*, "Heating rate and electrode charging measurements in a scalable, microfabricated, surface-electrode ion trap," *Applied Physics B* **107**, 913–919 (2012).
- <sup>31</sup>M. Cetina, A. T. Grier, and V. Vuletić, "Micromotion-induced limit to atom-ion sympathetic cooling in paul traps," *Physical review letters* **109**, 253201 (2012).
- <sup>32</sup>J. Bjorkholm, "Collision-limited lifetimes of atom traps," *Physical Review A* **38**, 1599 (1988).
- <sup>33</sup>M. Prentiss, A. Cable, J. Bjorkholm, S. Chu, E. Raab, and D. Pritchard, "Atomic-density-dependent losses in an optical trap," *Optics letters* **13**, 452–454 (1988).
- <sup>34</sup>M. Tomza, K. Jachymski, R. Gerritsma, A. Negretti, T. Calarco, Z. Idziaszek, and P. S. Julienne, "Cold hybrid ion-atom systems," *Reviews of modern physics* **91**, 035001 (2019).
- <sup>35</sup>R. Côté, "From classical mobility to hopping conductivity: Charge hopping in an ultracold gas," *Physical review letters* **85**, 5316 (2000).
- <sup>36</sup>A. Selin, A. Ermolaev, and C. Joachain, "Single ionization of the  $1\ 1\ s\ e$  and  $2\ 1\ p\ o$  states of he by  $1\text{-gev/u}$   $9\ 2+$  ions," *Physical Review A* **67**, 012709 (2003).
- <sup>37</sup>B. Zygelman, A. Dalgarno, M. Kimura, and N. Lane, "Radiative and nonradiative charge transfer in  $\text{he}^{++}$  h collisions at low energy," *Physical Review A* **40**, 2340 (1989).
- <sup>38</sup>B. Zygelman and A. Dalgarno, "Radiative quenching of  $\text{he}(2\ s\ 1)$  induced by collisions with ground-state helium atoms," *Physical Review A* **38**, 1877 (1988).
- <sup>39</sup>R. Gerritsma, A. Negretti, H. Doerk, Z. Idziaszek, T. Calarco, and F. Schmidt-Kaler, "Bosonic josephson junction controlled by a single trapped ion," *Physical Review Letters* **109**, 080402 (2012).
- <sup>40</sup>U. Bissbort, D. Cocks, A. Negretti, Z. Idziaszek, T. Calarco, F. Schmidt-Kaler, W. Hofstetter, and R. Gerritsma, "Emulating solid-state physics with a hybrid system of ultracold ions and atoms," *Physical Review Letters* **111**, 080501 (2013).
- <sup>41</sup>F. Schmidt-Kaler and R. Gerritsma, "Entangled states of trapped ions allow measuring the magnetic field gradient produced by a single atomic spin," *Europhysics Letters* **99**, 53001 (2012).